Surface Science 214 (1989) 111–140
North-Holland, Amsterdam

THE STRUCTURE OF A CLEAN AND OXYGEN COVERED COPPER SURFACE STUDIED BY LOW ENERGY ION SCATTERING

E. VAN DE RIET, J.B.J. SMEETS, J.M. FLUIT and A. NIEHAUS

Buys Ballot Laboratorium, Rijksuniversiteit Utrecht, Princetonplein 5, 3584 CC Utrecht, The Netherlands

Received 7 October 1988; accepted for publication 7 December 1988

The possible applications of the method of low energy ion scattering (LEIS) for the study of the structure of single crystal surfaces are critically analysed. Then LEIS is used to investigate a clean Cu(110) surface and its reconstruction upon adsorption of half a monolayer of O atoms. The main conclusions are as follows: (i) The distance between first and second layer atoms of the clean (110) surface is 0.04 Å smaller than the corresponding distance in the bulk. (ii) In the Cu(110)-(2×1)-O surface the oxygen atom is positioned in the long bridge position in the [001] surface row, 0.1 Å below the Cu atoms of the [001] surface row. (iii) The distance between [$\bar{1}$00] surface row containing the oxygen atoms and the second layer is 0.23 Å greater than a corresponding distance in the bulk. (iv) Every second [001] row is missing in the Cu(110)-(2×1)-O surface.

The distances between the oxygen and its nearest Cu neighbours in the reconstructed surface, calculated from the results (ii) and (iii), agree with direct measurements of these distances using the method of SEXAFS [5,6]. However, since the SEXAFS results were interpreted on the assumption of an unrelaxed first to second layer distance, the vertical oxygen position extracted from those data is at variance with our directly measured position.

1. Introduction

In this paper the atomic surface configurations of a clean Cu(110) surface and a Cu(110) surface with approximately half a monolayer of oxygen – the Cu(110)-(2 × 1)-O structure – are investigated. We apply the technique of low energy ion scattering (LEIS), which is an especially sensitive tool for the determination of atomic distances in the topmost surface layers. The shadowing of one atom by another can be measured easily as a sharp decrease in the ion scattering yield in a polar angular or azimuthal angular distribution.

The oxygen-covered surface has been studied by various methods over the last 10 years [1–13], after LEED (low energy electron diffraction) experiments have shown that this surface is arranged according to a (2 × 1) structure [14]. The first results concerning the position of the oxygen atoms in the surface were reported in 1979 by de Wit et al. [1] who applied the LEIS technique. In the mean time other surface sensitive techniques became available and existing techniques became more reliable such as SEXAFS (surface-extended X-ray absorption fine structure) and ICISS (impact collision ion scattering spectroscopy). The LEIS technique itself has also evolved as a result of improved measuring methods and the destructive influence of the technique has been minimised.

In spite of the fact that the Cu(110)-(2 × 1)-O surface has been subject of several recent studies in which these methods were used, there are still some unresolved problems. From recent SEXAFS measurements it is concluded that the oxygen atom is situated *above* the first surface layer, where as all LEIS measurements point to a position *below* the first layer. In the present study we will clarify this discrepancy.

We first give a historical survey of the results of previous studies; these show that a new investigation is needed. Then the version of the LEIS method that we used is described and critically analysed. Finally the results obtained for the clean Cu(110) and the Cu(110)-(2 × 1)-O surface are presented and discussed.

2. Historical survey

As stated in the previous section the clean and oxygen-covered Cu(110) surfaces have already been studied by de Wit and Bronckers [1,2] who made use of LEIS. In their first article on this subject, published in 1979, they found the oxygen to be positioned in the [001] surface row in the long bridge position, 0.6 ± 0.1 Å below the Cu atoms of the outermost layer. In determining this value they assumed an unreconstructed surface. Two years later, they showed that the adsorption of oxygen induces a recontruction in which every second [001] row of the outmost Cu layer becomes vacant [2]. In this second article the authors reported that the oxygen was 0.6 ± 0.2 Å below the first layer.

Although the conclusion of Bronckers and de Wit that the oxygen atoms occupy the long bridge position has been confirmed by many groups [3–13], there has been a divergency of opinion concerning the vertical position of the oxygen and the manner in which the copper surface is reconstructed. In the literature three models have been proposed for this reconstruction: (1) the missing row model (MR), as proposed in ref. [2], (2) the saw-tooth (ST) model in which not only every other [001] row of the first layer is missing, but also every second [001] row of the second layer, (3) the shifted row model (SR), in which every second [001] row of the first layer is shifted perpendicular to the surface.

Lapujoulade et al. [3,4] have studied the oxygen-covered surface with helium diffraction. In their first article on the subject [3] (1980) they stated that the oxygen atoms are 0.7 ± 0.1 Å below the surface, but they said nothing about a possible reconstruction of the surface. However, two years later [4] (1982) they supported the missing row model proposed by Bronckers and de Wit [2].

More recently, namely in 1984 and 1986, two SEXAFS studies have appeared on the subject [5,6]. SEXAFS measurements yield rather directly values for the distance between adsorbed atoms and their nearest neighbours. These distances are obtained from a comparison of a Fourier transform of electron spectra with calculated spectra. In this way Döbler et al. [5] found the distances between the adsorbed oxygen atoms and their two nearest neighbour copper atoms and confirmed that the oxygen atoms occupy the two-fold bridge site in the [001] row. The distance from an oxygen atom to the nearest first layer copper atoms of the [001] row was found to be 1.84 ± 0.02 Å and to the second layer atoms 2.00 ± 0.05 Å. Despite the fact that the SEXAFS technique does not yield information concerning the distance between the two topmost layers, the authors concluded that the position of the oxygen atoms was 0.35 Å above the first layer, on the assumption that the first interlayer distance equals the corresponding value in the bulk.

Two years later, data from another SEXAFS study were reported by authors from the same group (see Bader et al. [6] (1986)). They were able to obtain a value for the distance between the oxygen atoms and their two nearest neighbours more accurately, and to find out the distance between the oxygen atoms and the fourth nearest neighbour. They did not observe an intensity peak belonging to the third nearest neighbour observed in the Fourier transform of their spectra. From this fact, they concluded that the [001] Cu rows that do not contain oxygen atoms are missing. This absence of the third nearest neighbour rules out the SR model as a possible reconstruction model of the oxygen-covered surface. A SEXAFS amplitude comparison shows that the MR model is more likely to be the correct one than is the ST model. The distances found between oxygen atoms and their first and second nearest neighbours are listed in table 1, together with the corresponding values for the height of the oxygen above the first and second layer; again it is assumed that the distance between the first two layers (δ) equals the bulk value.

Table 1
Cu–O distances obtained from SEXAFS [6] measurements

Azimuth	Θ	Cu-neighbour	Cu–O distance (Å)	O above 2nd layer (Å)	O above 1st layer (Å)
[001]	90	1	1.82 ± 0.02		0.21 ± 0.21
$[\bar{1}10]$	90	2	1.99 ± 0.02	1.53 ± 0.03	0.25 ± 0.03
$[\bar{1}10]$	45	2	1.97 ± 0.02	1.50 ± 0.03	0.22 ± 0.03

The distances above the first layer are calculated, on the assumption of an unrelaxed surface.

Two groups have applied ICISS to the study of the oxygen-covered surface. Niehus and Comsa [7] (1984), using 2 keV Na^+ ions as projectiles, tried to find out whether the reconstruction is better described by an MR, ST or SR model. On the basis of a large number of ICISS data, they concluded that the MR model is the correct one.

ICISS has also been applied by Yarmoff et al. [8] (1986) to the study of the clean and oxygen-covered Cu(110) surface; they used 5 keV $^6Li^+$ ions as projectiles. Polar angular scans in the $[\bar{1}10]_s$, $[\bar{1}12]_s$ and $[001]_s$ azimuths were quantitatively analysed by comparing them to the results of Monte Carlo computer simulations. From these analyses they concluded that the distance between the first and the second copper layer of the oxygen-covered surface is relaxed by 0.32 ± 0.13 Å, and that the surface rearranges itself according to the missing row model. These values are the only ones we have found in literature for the relaxation of the oxygen-covered Cu(110) surface.

Döbler et al. [9] (1986) performed a NEXAFS (near-edge X-ray absorption fine-structure) study on the reconstruction of the oxygen-covered Cu(110) surface in an attempt to resolve between the three proposed reconstruction models. Their calculated and measured NEXAFS spectra show much better resemblance with each other for the MR model and the ST model than for the SR model. The authors stated that an equivocal resolution between the first two models must await further NEXAFS measurements.

The ST model was originally proposed by Bonzel and Ferrer [15] (1982) for the reconstructed Ir, Pt and Au(110)-(1 × 2) surfaces. In this model, the surface atoms have to move by only 2.8 Å in order to generate a 1 × 2 structure starting from a 1 × 1 structure. In the missing row model, the surface copper atoms have to move over distances large compared to the lattice distance to generate a 1 × 2 structure. However, the ST model for the Cu(110)-(2 × 1)-O surface has not been supported by any experimental evidence.

The adsorption of oxygen on Cu(110) has also been studied with high energy ion scattering by Feidenhans'l and Stensgaard [10] (1983). Good agreement between computer simulations and experimental data was obtained for an SR model in which every second [001] row is displaced outwards by 0.27 ± 0.05 Å from its bulk-like position. For the other [001] row no displacement was found within the error limit (0.03 Å). Calculations in terms of the missing row model, with inclusion of a relaxation, yield no acceptable agreement with the experimental data. Later on this SR model, in which the oxygen atoms occupy a position in the [001] row, was supported by the results of angle resolved ultraviolet photoemission spectroscopy (ARUPS) (see Didio et al. [11] (1984)).

Because of the large disagreement between the results obtained by the various groups mentioned in the previous paragraphs, we have done a new LEIS study on this subject. No one disagrees with the conclusion that the

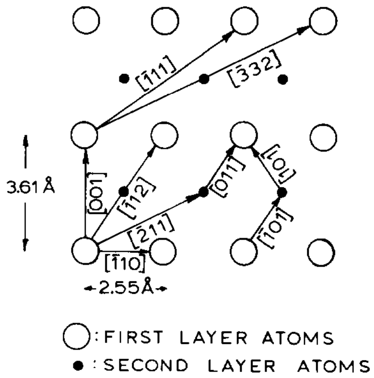

Fig. 1. Schematic top view of the atoms in the first and second layer of a Cu(110) crystal. The large circles represent the Cu atoms in the first layer and the black dots the second layer copper atoms. The main crystallographic directions are indicated together with their Miller indices.

position of the oxygen atoms is in the [001] row, so we will not discuss the evidence for this. We will discuss only our results concerning the relaxation of the clean surface, the reconstruction and relaxation of the oxygen-covered surface and the height of the oxygen atoms above or below the surface.

In the following sections, some preliminary remarks concerning the experimental set-up will be followed by a discussion of the LEIS method and its accuracy. This method will be applied first of all to the clean surface and secondly to the oxygen-covered surface, in order to obtain information about the atomic surface configuration. Finally we will show that although our results are not in conflict with the SEXAFS [5,6] and ICISS [7,8] measurements, they do lead to an interpretation which is in disagreement with the interpretation derived from the SEXAFS results.

3. Experimental

The copper single-crystal rod, purchased from Metal Crystal&Oxides Ltd., Cambridge, England, was oriented with Laue X-ray diffraction and was spark cut from a cylinder of a single crystal with 5N purity. A sample with a thickness of 3 mm and a diameter of 13 mm was polished mechanically and electrolytically and finally mounted on a crystal manipulator.

The experimental set-up has been described before (see van Zoest [16]). A survey will be given here. A schematic drawing of the apparatus is given in fig. 2. The UHV chamber has a base pressure of 2×10^{-10} Torr. During the ion scattering experiments, the pressure rises to about 1×10^{-9} Torr, due to the higher gas pressure in the ion source. Because we used only noble gas ions as

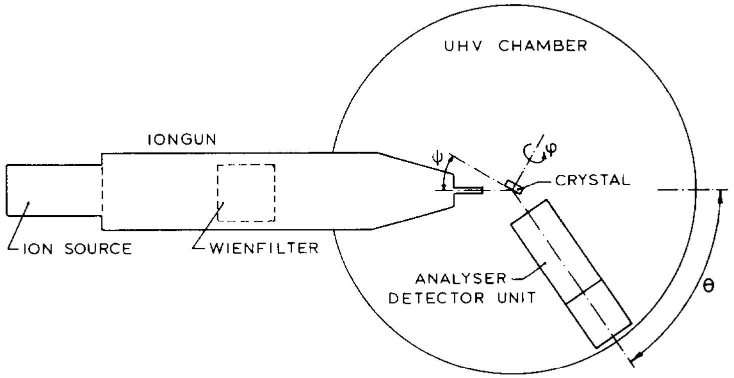

Fig. 2. Schematic side view of the apparatus. The analyser detector unit can also turn out of this plane from $\Delta = 0°$ to $\Delta = 90°$.

projectiles for the experiments described below, this pressure increase does not increase the contamination rate of the copper surface.

The ion source produces a beam with a typical current of 20–100 nA, depending on the projectile energy (2–5 keV). The beam has a diameter of 1 mm and an angular divergence of $< 1°$. The Wien filter is used to separate the $^{20}Ne^+$ ions from H_2O^+ and $^{22}Ne^+$ ions.

With the crystal manipulator we can vary the polar angle of incidence (ψ), also called angle of incidence, and the azimuthal angle of incidence (ϕ), also called azimuthal angle. The angle ψ can be varied between 0° and 180°, is reproducible to within 0.1° and has an absolute accuracy of 0.3°. The angle ϕ can be varied over more than 360° with the same reproducibility and accuracy as ψ. The analyser can be rotated in and out of the plane of incidence. This plane is defined by the incoming ion beam and the surface normal. In the plane of incidence, the analyser can be varied from $\Theta = 0°$ to $\Theta = 120°$ with respect to the ion beam. Rotation out of this plane is possible from $\Delta = 0°$ to $\Delta = 90°$ around a vector lying in the plane of incidence and forming an angle $\Theta - \pi/2$ with the beam. The observation direction of the detector is thus given by the vector $(\sin(\Delta), \cos(\Delta)\sin(\Theta), \cos(\Delta)\cos(\Theta))$, the z-axis being defined by the beam and the plane of incidence being the yz plane.

The scattered ions are energy analysed with a double flat-plate analyser. Its energy resolution is 4%, its acceptance angle in the plane of incidence is 2° and out of it 4°.

We also have the possibility to measure energy spectra using a TOF technique. In this detection mode the primary beam is chopped by deflection plates, and energy spectra of scattered ions and/or neutrals are obtained from a measurement of their flight time from the crystal to the detector, which is positioned at a distance of 220 mm from the crystal.

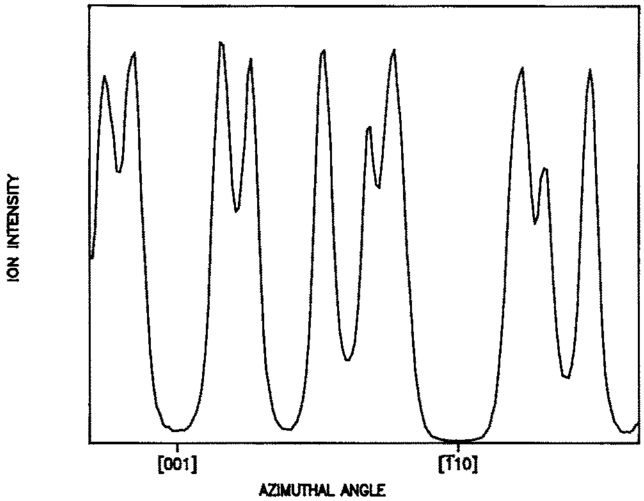

Fig. 3. Azimuthal angular distribution of a clean copper surface with $\psi = 8°$, $\Theta = 90°$, $\Delta = 0°$, obtained with 5 keV Ne^+ projectiles.

The copper sample was cleaned in the UHV chamber with cycles of 5 keV neon ion bombardment followed by annealing up to 600 °C. We regarded the copper surface as clean if two criteria were met. The first criterion was that, upon bombardment with 5 keV neon ions, the energy peak belonging to negatively charged oxygen recoil ions measured at $\Theta = 40°$ and $\Delta = 0°$ had decreased to a value of less than 1% of the value obtained for a surface with a monolayer of oxygen. This is a guarantee that the oxygen coverage is smaller than 1%. The second criterion was that the ratio of the maximum and the minimum intensity of scattered ions in an azimuthal distribution with $(\psi, \Theta, \Delta) = (8°, 90°, 0°)$ for 5 keV primary neon ions was larger than 100. Such an azimuthal angular ion distribution is shown in fig. 3. This procedure guarantees that the surface is clean and well ordered.

All the azimuthal angular and polar angular ion distributions are measured in the following way. First of all the energy position of the "quasi-single" scattering peak is determined. To do this, we aim the beam along the $[\bar{2}11]$ crystal direction so that the second and deeper layer atoms are in the shadow of the first layer atoms, and measure an energy spectrum. For an example see fig. 4. To determine the quasi-single scattering peak of the negatively charged oxygen recoil ions, we aim the beam in such a direction that the oxygen atoms on the surface are not shadowed by other surface atoms. The energy position of the maximum ion intensity in such a spectrum is taken as the quasi-single peak position. In this way the influence that the double scattering exerts on the determination of the position of the quasi-single scattering energy is

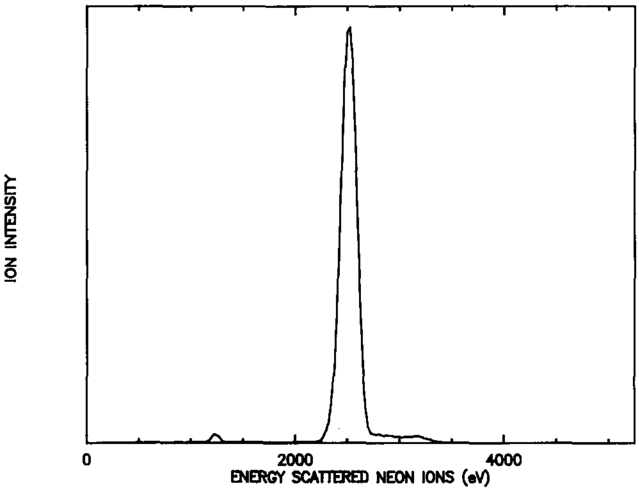

Fig. 4. Typical energy spectrum of neon ions with a primary energy of 5 keV with $\Theta = 90°$ and $\Delta = 0°$ and with the beam aimed along the $[\bar{2}11]$ direction.

minimised. For measurements of angular distributions, the energy of the analyser is set to a value corresponding to the quasi-single peak value.

The neutral azimuthal and polar angular distributions are measured in a similar way. First of all a time-of-flight spectrum is made, again with the beam directed along a suitable crystal direction. The position of the quasi-single peak in this TOF spectrum is determined. A time window with a width of 100 ns is set around the quasi-single peak. In measurements of angular distributions, the only particles to be counted are those that reach the detector in the above-mentioned time interval.

To correct for the tilt in the crystal, all the polar angular distributions are measured twice, at azimuthal angles differing by 180°. Due to the tilt, the two polar angular distributions measured in this way are shifted on the ψ scale in relation to each other. This shift is equal to or less than twice the tilt in the crystal. The tilt is caused by the fact that the crystal is not cut exactly perpendicular to a $\langle 110 \rangle$ row and by the fact that the crystal normal is not precisely aligned along the rotation axis of the azimuthal angle. The tilt of our copper crystal due to these two effects was $0.7 \pm 0.1°$.

The polar angular distributions shown in this paper are all corrected for a trivial geometry effect which is explained below. In first order, when we neglect shadowing, blocking, focusing, neutralisation and other phenomena, the intensity of scattered particles observed in a certain direction is proportional to the number of unit cells that are seen by the beam and by the detector, i.e. the intensity is proportional to the area of that part of the beam spot on the surface, from which the scattered particles can reach the detector.

For large ψ, when the detector sees the whole beam spot on the crystal, we can correct for this effect by multiplying each data point by $\sin(\psi)$. For smaller ψ, $\psi \leq 15°$, depending on Θ, the correction depends on the shape of the beam spot and on the area seen by the detector. Uncertainties regarding these quantities make it uncertain which correction function should be applied. When we retrieve information from intensity steps in polar distributions, the possible systematic error induced in this way in the angular position of these steps as determined from the measured distributions, depends on their width and their angular position. In the present study we estimate this possible systematic error to be less than 0.4°.

The distributions of the oxygen covered surface are measured with a background pressure of 5×10^{-8} Torr oxygen. A few of these distributions are compared to distributions taken with the crystal prepared in the way Yarmoff et al. [8] have described. In this method, the crystal is exposed to 200 L oxygen and afterwards annealed at 100 °C for 5 to 10 min. Within the experimental uncertainties, the critical angles obtained in these two ways do not differ from each other. The advantage of measuring with a background pressure is that time-consuming re-exposure to oxygen and reannealing of the crystal are avoided.

An extensive explanation of the shadow cone model is given by Mashkova and Molchanov [17]. This model will not be further discussed in this paper. All the spectra relevant to this article are taken with neon ions as projectiles.

4. Method and data analysis

4.1. Choice of projectile, projectile energy and geometric configuration

In the past, many authors have stated that noble gas ions are not suitable for use in an accurate LEIS analysis of a surface. The neutralisation probability would be too high and would change strongly with a small variation in the angle of incidence. As a result, high doses would be necessary which would influence the sample, and structures in the polar angular distributions would be distorted or smoothed and thus an accurate evaluation in terms of surface geometry would be prevented.

The above arguments may be partly correct for helium ions, but we will show below that neon ions are very well suited for accurate LEIS analysis, provided that the primary energy and scattering angle chosen are appropriate.

To find out the optimum conditions for neon ions as projectiles for a LEIS study of the Cu(110) surface, we investigated the influence of the scattering angle and projectile energy on the relevant LEIS signals. In fig. 5, polar angular distributions measured in the $[\bar{1}12]_s$ azimuth at various scattering angles are presented. For scattering angles larger than 70°, a sharp surface

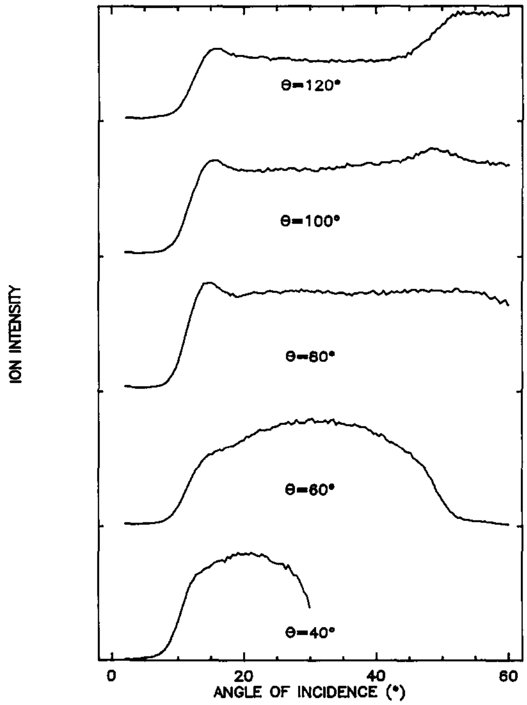

Fig. 5. Polar angular distributions measured in the $[\bar{1}12]_s$ azimuth at various scattering angles Θ with 5 keV Ne^+ projectiles, $\Delta = 0°$.

shadow edge, including a small focus peak, is observed. For smaller angles, the focus peak disappears and the shadow edge becomes less steep. For large scattering angles, e.g. the $\Theta = 120°$ distribution in fig. 5, an almost constant ion yield is found between the two shadow edges. This indicates that the ion fraction and thus the neutralisation probability does not change much within the relevant range of polar angles.

Similar behaviour is observed if one measures polar angular ion distributions again, but now for different projectile energies at $\Theta = 120°$ (fig. 6). These distributions are taken in the $[001]_s$ azimuth. Above 4 keV a sharp shadow cone edge is observed whereas below 3 keV, the intensity rises only very slowly with increasing angle of incidence.

Polar angular distributions for the same primary energies and azimuthal angle were also measured in the TOF mode; both scattered ions and neutrals were counted. For 4 keV and higher energies, these distributions show sharp shadow edges which agree in slope and position, within 0.2°, with the corresponding ones of the distributions of fig. 6. For lower energies the TOF polar angular distributions still have steep shadow edges, in contrast to the ion

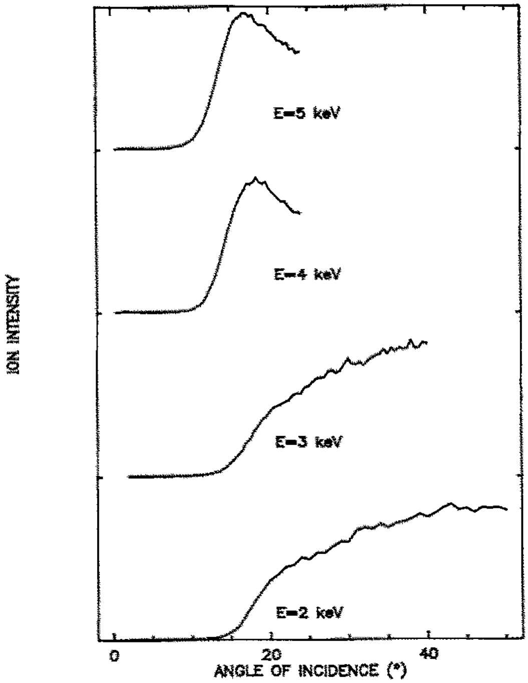

Fig. 6. Polar angular distributions measured in the $[001]_s$ azimuth for primary energies between 2 and 5 keV, $\Theta = 120°$, $\Delta = 0°$.

polar angular distributions. In this case, comparison of the angular positions of the shadow edge is not possible, because they do not have the same shape.

These phenomena can be understood if the ion fraction of the scattered neon is taken into account. This quantity can be measured directly in the TOF mode. Its dependence on the projectile energy at constant angles Θ, Δ, ψ and ϕ is shown in fig. 7a, and its dependence on the scattering angle Θ at constant (ϕ, Δ, ψ) and projectile energy is shown in fig. 7b. From these figures it is clear that conditions characterised by a large ion fraction lead to sharp shadow edges in polar angular distributions (see figs. 5 and 6), i.e. large scattering angles and high primary energies.

A profound discussion about the neutralisation phenomena will be published in the near future. In the present paper on surface structure determination, it is sufficient to conclude phenomenologically, from figs. 5–7, that neon scattering can very well serve as a tool for investigating the geometrical structure of a copper surface. Under suitable conditions, the ion fraction is large enough to allow the necessary information to be obtained using low numbers of incoming particles, comparable to the numbers needed in the case of alkali primary ions. In addition, the position of the shadow edges are not

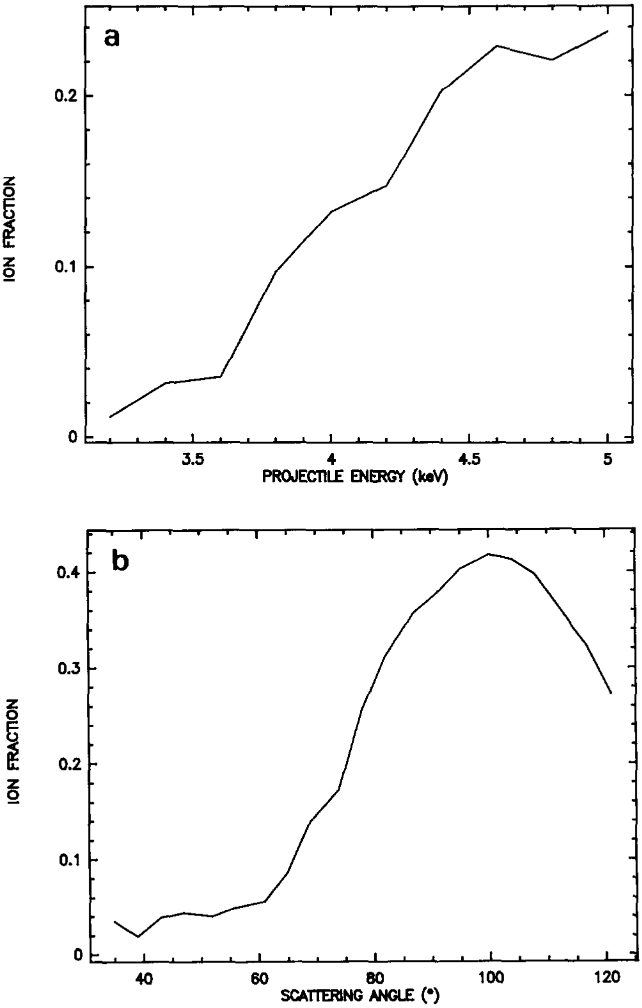

Fig. 7. Ion fraction of the scattering neon particles as a function of (a) projectile energy at $\Theta = 120°$ and (b) scattering angle, the primary energy is 5 keV. $\Delta = 0°$ and $\psi = 8°$ for both plots.

distorted by neutralisation effects. Consequently, the analysis of our spectra can be performed with classical mechanics alone, without taking neutralisation phenomena into account.

An advantage of the sharp decrease in the ion fraction if the scattering angle or the projectile energy is decreased is the insensitivity of our ion yield to multiple scattering processes. If the last scattering angle in such a multiple scattering process is smaller than 70° or if the energy of the neon before the last scattering is smaller than 3 keV, the chance that the neon will leave the surface in an ionised state will be low. Alkali metals do not behave like this. For this reason too, neon is a better tool for investigating the two topmost layers of a copper surface than are alkali metals.

We also tried to use He^+ projectiles within the energy range, from 2 to 5 keV, the range accessible with our apparatus. The ion fraction was found to be less than 2% over the whole range at all scattering angles, and the polar angular distributions did not show sharp shadow edges. This rules out helium ions as a good choice of projectile for LEIS studies of surface structure with our apparatus, at least as far as the detection of scattered ions is concerned.

The characteristics of alkali scattering are comparable to those of noble gas scattering when neutralised noble gas particles are counted. The advantage of these two types of scattering over noble gas ion scattering is that lower doses can be used. However the main disadvantage is its relatively low surface sensitivity. This is a particular disadvantage if one wants to determine the relaxation of the surface layers, because the corresponding shadow structures in the measured distributions will always be a superposition of slightly shifted structures from which the contributions belonging to the first and second layer cannot usually be easily retrieved.

The above outlined differences between ion and neutral detection are demonstrated in fig. 8. In this figure, a neutral particle and an ion distribution are shown. These distributions are measured under the same conditions, in the $[001]_s$ azimuth with $(\Theta, \Delta) = (90°, 0°)$. In the neutral particle distribution one sees clearly the shadow of the first layer atoms on the third layer atoms in

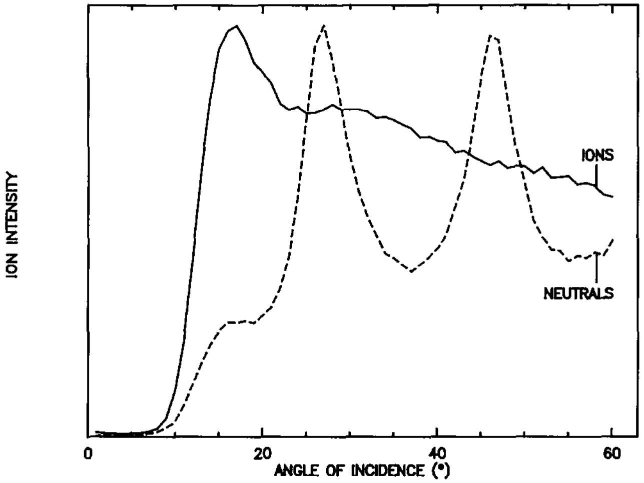

Fig. 8. Two polar angular distributions in the $[001]_s$ direction, $\Theta = 90°$, $\Delta = 0°$ and the primary energy is 5 keV. The dashed line shows the neutral scattering yield and the solid line shows the ion scattering yield.

the $[\bar{1}\bar{1}2]$ direction. This shadow can be seen as the dip around $\psi = 35°$. This dip is absent in the ion distribution, so one can conclude that the third layer does not contribute to the ion yield. The positions and the widths of the [001] surface shadow edge of these two distributions are equal. This shows that one can analyse the polar angular distributions without taking neutralisation phenomena into account.

In order to get reliable results concerning the relaxation of the surface we will use ion yields to which the third and deeper layers do not contribute.

All spectra in the remainder of this paper are ion spectra, obtained with a 5 keV neon$^+$ primary ion beam.

4.2. The analysis of the polar angular distributions

Now that we have concluded that under suitable conditions, the analysis of the polar angular distributions can be performed with classical mechanics alone, we will briefly discuss how the distributions can be interpreted on the basis of a three-particle model. With this model, we study what happens if an energetic neon projectile, with an impact parameter b with respect to the first of two copper atoms, is scattered by two copper atoms separated by a distance d, in the case where the vector of initial velocity of the projectile lies in the plane defined by the three particles. The angle between the beam and the line connecting the two copper atoms is called α (see fig. 9). Computer calculations in two dimensions based only on classical dynamics yield the relation between α, d, b and the total scattering angle Θ. We have used the inter-atomic potential proposed by Fauster and Metzner [18]. This is a Moliere potential in which the screening length is reduced by a factor 0.7.

The computer calculations are based on a numerical integration of the equations of motions. At every point of the trajectory, the forces on the three

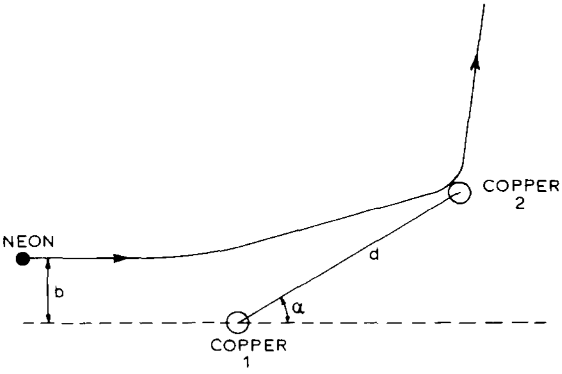

Fig. 9. Possible trajectory of an incident neon ion, with an impact parameter b with respect to the first copper atom, scattered by two copper atoms separated over a distance d. The angle between the beam direction and the line connecting the two copper atoms is defined as α.

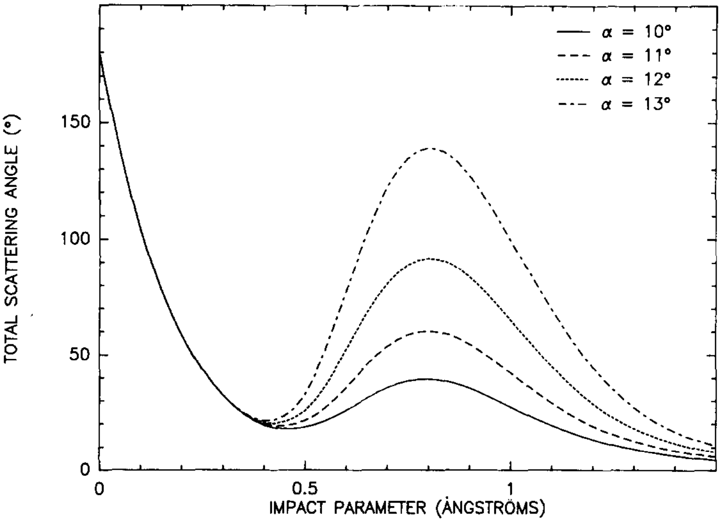

Fig. 10. Total scattering angle of a 5 keV neon atom scattered by two copper atoms for various values of α. The maximum on the right side of each graph is defined as the critical angle $\Theta_c(\alpha)$. The initial distance between the two copper atoms is 4.42 Å.

particles involved are calculated, using the Moliere potential. From these forces, the velocity changes of the particles are calculated and from these velocities one can calculate the changes in the position of the three particles.

In fig. 10 the thus calculated total scattering angle of the incident neon atoms is drawn as a function of impact parameter for various values of α and for constant initial distance d between the two copper atoms. For small values of b, the scattering angle does not depend on α. In this region, the influence of the second copper atom on the scattering process is negligible. For larger b, the role of the second copper atom can be large if α is sufficiently large. For small α, the second atom is in the shadow cone of the first atom, so the neon atom cannot approach the second atom closely, which prevents strong scattering. With increasing α, the neon can be scattered by the second copper atom over increasing scattering angles. The value of α for which scattering over an angle Θ is possible depends on d. From fig. 10 one can define a critical angle Θ_c as a function of α, the maximum angle over which a neon ion can be scattered mainly due to interaction with the second copper atom. The value of this critical angle is given by the maximum of the corresponding $\Theta(b)$ curve shown in fig. 10.

The relation $\Theta_c(\alpha)$ can be inverted to $\alpha_c(\Theta)$, with α_c the angle between the beam and the line connecting the two copper atoms, which is necessary to scatter the neon over an angle $\Theta = \Theta_c$. This relation is more useful, since the polar angular distributions are always measured at a constant scattering angle.

Table 2
Comparison of the critical angles of surface shadows in polar angular distributions with the calculated values, for four different surface shadows

Θ	d = 2.556 (Å) [$\bar{1}$10]				d = 3.615 (Å) [001]				d = 4.427 (Å) [$\bar{1}$12]				d = 5.112 (Å) [$\bar{1}$10]			
	M	C	M − C	ES	M	C	M − C	ES	M	C	M − C	ES	M	C	M − C	ES
120	18.1	16.8	1.3	4.5	13.2	13.0	0.2	3.4	11.4	11.2	0.2	2.8	10.3	10.1	0.2	0.3
100	18.2	16.3	1.9	5.2	12.8	12.7	0.1	3.8	11.0	10.9	0.1	3.2				
80	17.1	15.6	1.5	5.4	12.3	12.2	0.1	3.8	10.5	10.5	0.0	3.2				

(M) Measurement (deg); (C) calculated value (deg); (ES) calculated energy shift (%) of the final projectile energy at the edge of the shadow cone. The d = 5.112 shadow edge is measured on an oxygen-covered surface, in which the distance between two surface copper atoms in the [$\bar{1}$10] direction is twice the bulk value.

If one considers a shadow of one surface atom on another surface atom, the angle $\alpha_c(\Theta)$ is the same as the critical angle of incidence ψ_c. In the calculations, the angle α is varied until Θ_c equals the experimental scattering angle. The α_c thus found can be compared directly to the experimental value $\psi_{c,exp}$. A simple goniometric relation holds for shadows of a surface atom on a second layer atom. This relation depends on various parameters such as the distance between the first and second layer.

In the region of a critical angle, the scattering process takes place mainly, but not fully, due to the second copper atom. The incoming neon projectiles are first scattered by the first copper atom over a few degrees, depending on the distance between the two scatterers, before the strong scattering by the second copper atom takes place. As a result, the value of the final energy of the neon deviates from the energy position of the quasi-single energy peak. This energy shift will be discussed later on.

In table 2, the critical angles calculated in this way are compared to the corresponding angular position of an edge of a surface shadow in a polar angular distribution. The position of an edge is defined as the position of the half-height of the slope. This choice is somewhat arbitrary. Aono [19] has proposed instead to take the 70% height between the background intensity and the maximum intensity, and Hetterich et al. [20] have proposed to take 80%. We chose the 50% value because at this height the slope of an intensity distribution is at its maximum, which lets the position of a step be determined the most accurately.

The calculated values differ only slightly from the experimental ones. This shows that we are able to calculate the position of a shadow edge very accurately, especially for distances larger than 3.6 Å.

The aim of the calculations is not only to show that we are able to predict the position of a surface shadow edge in a polar angular distribution but is primarily to find a value for the relaxation of the surface. To estimate the distance δ between the first and the second layer, a polar angular distribution is taken around a shadow of the first layer atoms on the second layer atoms. The critical angle $\psi_{c,exp}$ found experimentally together with δ, the distance between the two topmost layers, determines the critical angle α_c used in the calculations (see eq. (1)). The distance d between the two copper atoms involved depends only on δ:

$$\alpha_c = \psi_{c,exp} - \arcsin(\delta/d) + s. \qquad (1)$$

In this equation, s represents the difference between the experimental critical angle and the calculated one of a surface shadow edge over approximately the same distance and the same scattering angle as the edge under study. The value of s is equal to the value of M − C, listed in table 2, of the corresponding shadow. From the experimentally determined critical angle $\psi_{c,exp}$

and the experimental scattering angle, the unknown distance δ is obtained as follows:

(i) from the simple geometrical relation (1), the critical angle α_c is calculated for an assumed δ;

(ii) for the same δ, using the value for α_c just obtained, the critical scattering angle Θ_c is calculated;

(iii) δ is varied till the calculated scattering critical angle is equal to the experimental one.

We made use of the potential proposed by Fauster and Metzner [18]. Many other potentials have been proposed in the past. Our choice was guided by the excellent agreement between our calculations and our experimental results.

5. Results concerning the surface structure

5.1. The relaxation of the clean Cu(110) surface

To get a general idea of the clean Cu(110) surface, we made a photogram (fig. 11). In a photogram, the intensity of scattered ions is given as a function of the azimuthal angle ϕ (x-axis) and the polar angle ψ (y-axis). In fig. 11 approximately circular white areas of low ion intensities – the shadows – are

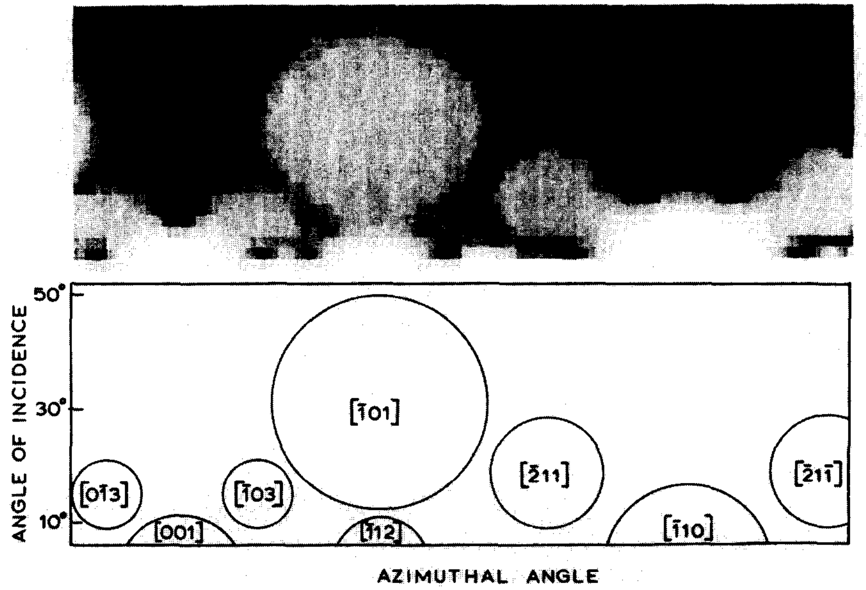

Fig. 11. Photogram of a clean copper surface, $\Theta = 120°$ and $\Delta = 0°$. The most important shadow cones are redrawn schematically in the plot below.

clearly visible. One can easily see which shadows have sharp edges; these are the edges whose position can be determined accurately.

It takes one second to measure one data point and more than an hour to measure the whole photogram. Unfortunately, both the beam intensity and the channeltron efficiency are not constant over such a long time. To obtain reliable results, we applied the following procedure. A series of azimuthal

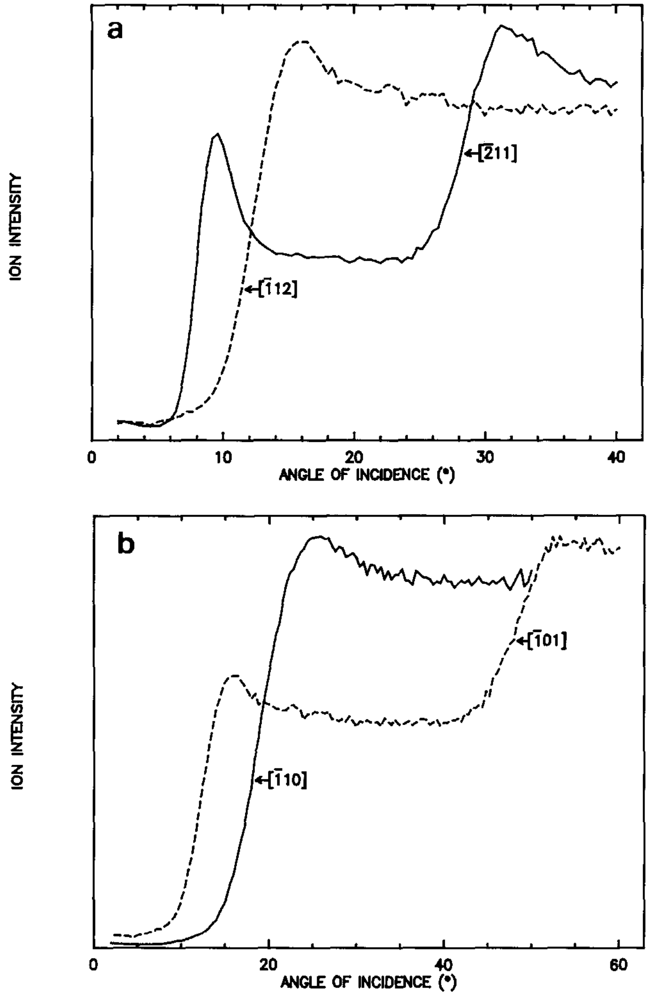

Fig. 12. Comparison of a surface shadow with a shadow of the first layer on the second layer over almost equal distances, $\Theta = 120°$ and $\Delta = 0°$. In (a), the upper graph, a comparison is made between the $[\bar{2}11]$ shadow edge and the $[\bar{1}12]$. In (b), the lower graph, a comparison is made between two $\langle 110\rangle$ shadow edges.

Table 3
Comparison of critical angles for various shadows and the relaxation derived from these angles

Θ (deg)	ψ_c $[\bar{2}11]$ (deg)	ψ_c $[\bar{1}12]$ (deg)	$\delta - \delta_0$ (Å)	ψ_c $[\bar{1}01]$ (deg)	ψ_c $[\bar{1}10]$ (deg)	$\delta - \delta_0$ (Å)
120	27.6 [a]	11.4 [a]	−0.05	47.6 [a]	18.1 [a]	−0.03
100	27.4	11.0	−0.03			
80	26.7	10.5	−0.05			

δ_0 represents the bulk value.
[a] See fig. 11.

distributions, the building blocks of a photogram, is taken within a selected range of polar angles of incidence. In addition a few polar angular distributions are taken and used to calibrate the individual azimuthal angular distributions with respect to each other. In this way, variations in the beam intensity and channeltron efficiency play only a minor role. The photogram is also corrected for the ψ dependence of the area of the beam spot on the surface seen by the detector.

To obtain a value for the distance between the two topmost surface layers (δ), the $[\bar{1}12]$ shadow edge is compared to the $[\bar{2}11]$ edge and the $[\bar{1}10]$ edge to the $[\bar{1}01]$ edge, at various scattering angles. The results are listed in table 3. Some of these distributions are drawn in fig. 12. The detector is positioned in the plane of incidence and the projectile energy is 5 keV.

The $[\bar{1}10]$ shadow and the $[\bar{1}01]$ shadow cannot be compared at smaller scattering angles than 110° because of a blocking effect in the [011] direction.

The rather extended calculations described above are not necessary to derive the relaxation, if the two $\langle 112 \rangle$ shadows are compared. We found that if the simple relation (2) is used, the same values are obtained for the relaxation $\delta - \delta_0$.

$$\delta - \delta_0 = 4.43(\sin(\Delta\psi) - \sin(16.77))\ \text{Å}. \tag{2}$$

The length of the $[\bar{2}11]$ vector is 4.43 Å and the angle between the $[\bar{2}11]$ vector and the surface is 16.77°. $\Delta\psi$ is the difference in the critical angles. This formula can be applied to this set of shadows, because the distance between the two copper atoms in the $[\bar{2}11]$ direction hardly depends on a small relaxation of the distance between the first layer and the second one. The more extended calculations are needed if a comparison is made between the $[\bar{1}01]$ shadow and the $[\bar{1}10]$ shadow, because a possible relaxation significantly changes the distance between the copper atoms in the $[\bar{1}01]$ direction.

The internal consistency is very good, as can be seen in table 3. The variations in the value for δ, obtained from our distributions are less than 0.02 Å. However, the absolute uncertainty is larger.

An estimate of this absolute uncertainty has been made. The main contributions to this error are: (1) statistical uncertainty (0.2°); (2) absolute accuracy of the angles (0.3°); (3) uncertainty in the way the distributions need to be corrected for the size of the beam spot seen by the detector ($< 0.4°$, depending on ψ). The total error caused by these three effects is $< 0.5°$. It can be concluded that the distance between the first and second layer of the clean Cu(110) surface is reduced by 0.04 ± 0.04 Å or (3 ± 3)%.

We also considered the possible influence of the difference in the shape of the steps in the polar angular distributions used for the determination of δ. In the case of different step width, an error might be introduced if the 50% value of a step is not an appropriate measure of its position. To get an estimate of this effect, we determined the angular distance between the steps in the $[\bar{1}10]$ and $[\bar{1}01]$ direction, using the 1/3 and 2/3 value of the step height respectively. The difference in the angular distance obtained using these two criteria ($\mathrm{D}\Delta\psi$) can be taken as an upper limit of the possible error that might be introduced if the 50% criterion were not appropriate. In our experiments we obtain $\mathrm{D}\Delta\psi < 0.2°$, which is much smaller than the possible error estimated above.

A significant difference could be caused by a difference in the Debye temperature of the two topmost layers, or by mixing of two neighbouring shadows.

In our model it has been assumed that the incoming neon ions are scattered by only two copper atoms. It is necessary to estimate whether deflection by a third copper atom is indeed negligible. This deflection is largest if the $[\bar{2}11]$ shadow is studied. The nearest copper atom in the $[\bar{1}10]$ direction relative to the first copper atom deflects the incident neon particles at the edge of the shadow cone more than the other copper atoms do. However, we have

Table 4
Survey of the results on the relaxations for the clean Cu(110) surface obtained by various techniques and authors

Technique	Authors	Δd_{12} (%)	Δd_{23} (%)
LEED	Adams et al. [21,22]	-8.5 ± 0.6	2.3 ± 0.8
	Davis et al. [23]	-10.0 ± 2.5	0.0 ± 2.5
	Noonan and Davis [24]	-8 ± 3	
	Davis and Noonan [25]	-10.0 [a]	1.9
		-7.9	2.4
		-9.5	2.6
HEIS	Stensgaard et al. [26,27]	-5.3 ± 1.6	3.3 ± 1.6
MEIS	Copel et al. [28]	-7.5 ± 1.5	2.5 ± 2.5
ICISS	Yarmoff et al. [8]	-10 ± 5	
	Fauster [29]	-10 ± 3	8 ± 6
LEIS	This work	-3 ± 3	

[a] Depending on the choice of the type of R-factor analysis.

calculated that this extra deflection is only 0.5° and mainly directed parallel to the surface. Because the shadow cone is approximately circular, this deflection influences the experimentally found critical angles by much less than the above-mentioned 0.5°. This extra error can thus be neglected. If the same shadow is studied on the oxygen-covered surface, and if this surface is reconstructed according to the missing row model or to the saw-tooth model, the nearest neighbour in the $[\bar{1}10]$ direction is absent. Deflection by all other atoms is much weaker, so we can neglect this effect altogether.

Our results can be compared to results published previously. Table 4 clearly shows that our value for the relaxation is the lowest of the values obtained by various techniques. The difference between our results and those of Fauster [29] is especially remarkable, because Fauster's results were also obtained with 5 keV neon projectiles. The other ion scattering techniques are in agreement with our results within the error. The LEED measurements, however, deviate from our results by twice the error.

5.2. *The reconstruction and the relaxation of the oxygen-covered surface*

Two photograms were made in order to get an overview of the oxygen-covered copper surface structure. The first photogram (fig. 13a) represents the scattered neon ions detected at a scattering angle $\Theta = 120°$. There are many differences between this photogram and the one shown in fig. 11. In fig. 13a, a shadow around the $[\bar{1}00]$ direction can easily be distinguished. This shadow indicates than neon ions scattered by the third layer copper atoms can reach the detector in an ionised state. The photogram of the oxygen covered surface is somewhat fainter. The main reason for this is that the third layer is visible. Because the first interlayer distance is not equal to the second one, two slightly shifted shadows, one of the first layer on the second and one of the second layer on the third, cause one faint shadow in the photogram.

An O^- recoil photogram, $\Theta = 55°$, is shown in fig. 13b. At least three areas of low intensity can be distinguished. A large shadowing and blocking region in the $[001]_s$ direction is observed; thus confirming the conclusion that the oxygen atoms are in the [001] row where the large shadows and "blocks" of the two neighbouring copper atoms prevent a recoil signal from being observed. The two other clearly distinguishable regions are caused by the shadow of oxygen atoms on oxygen atoms in the $[\bar{1}10]_s$ direction, and by the shadow of copper on oxygen atoms in the $[\bar{2}21]_s$ direction. The latter shadow will be used to determine the height of the oxygen above or below the surface.

The procedure used to determine the relaxation of the clean surface cannot be applied to the oxygen-covered surface without modification. It can be applied only if the third layer does not contribute to the ion yield; according to the photogram (fig. 13a), this is not the case with the oxygen-covered surface. The experimentally found $[\bar{2}11]$ shadow edge does indeed appear to be

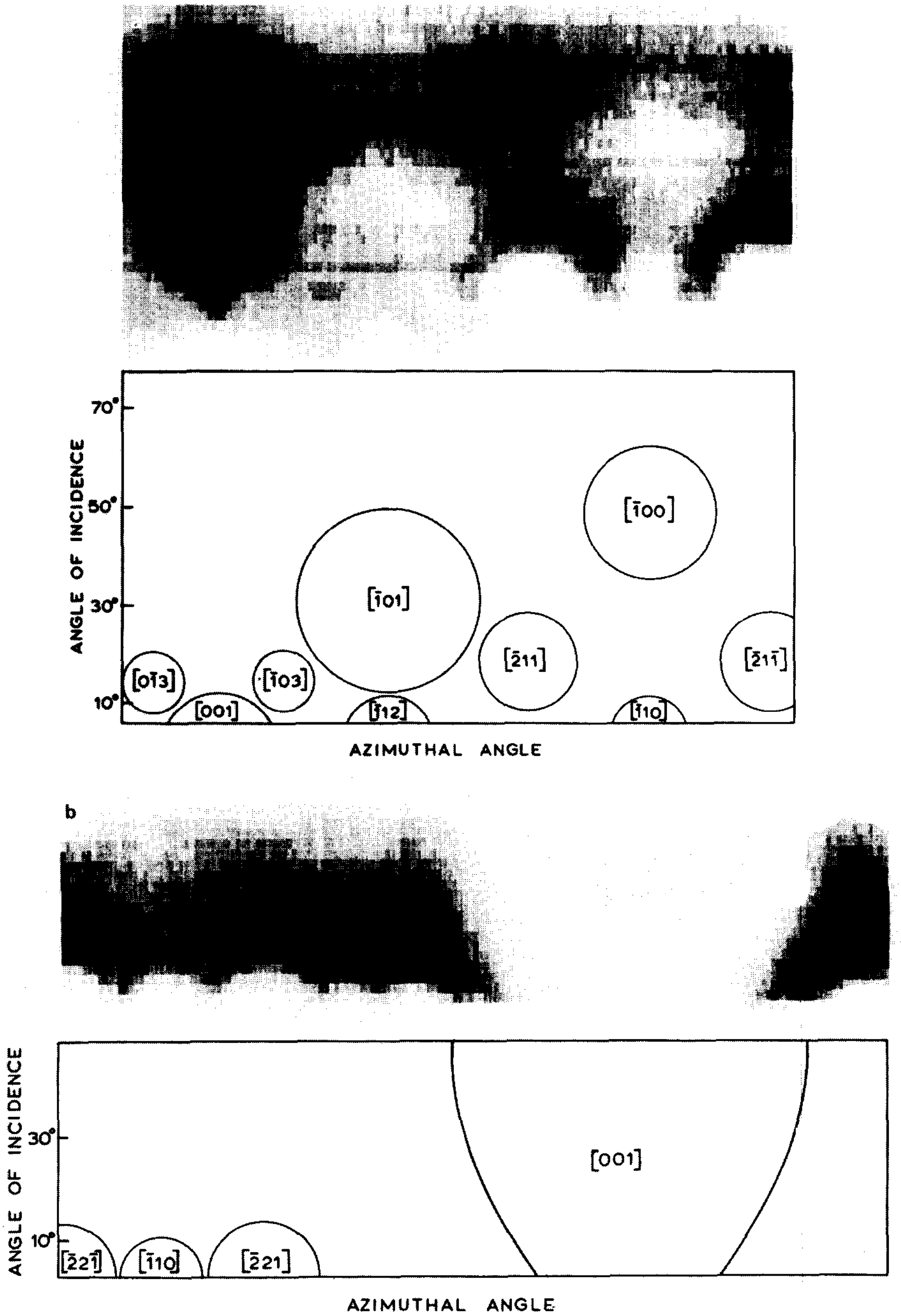

Fig. 13. Two photograms of the oxygen-covered surface. The upper one was measured while reflected neon ions were being counted at $\Theta = 120°$ and the lower one was measured while negatively charged oxygen ions were being counted at $\Theta = 55°$ and $\Delta = 0°$.

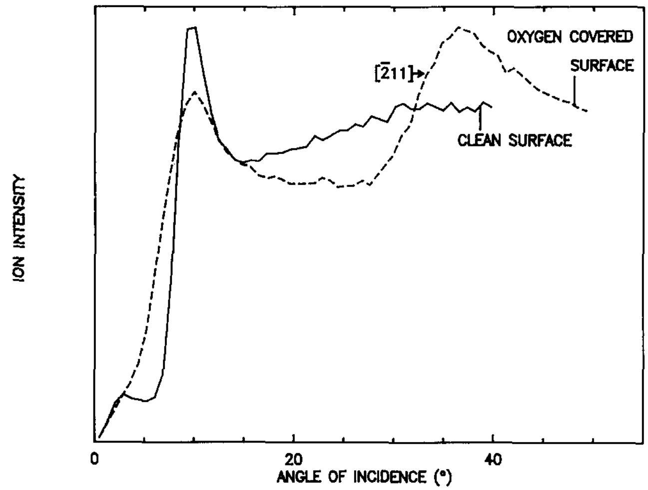

Fig. 14. Two polar angular scans in the $[\bar{3}32]_s$ direction with the detector placed in the [101] blocking direction, $\Theta = 124°$ and $\Delta = 59°$. The solid curve shows the distribution for the clean surface and the dashed line shows the distribution for the oxygen covered surface. The solid line exhibits no sharp edge at $\psi = 32°$, in contrast to the dashed line.

broadened. The difference in the angular position of the 1/3 and 2/3 height for this shadow edge is 2.0°, compared to 1.3° for the same shadow edge on the clean surface. If the oxygen-covered surface is reconstructed according to the missing row model, there will be twice as many third layer atoms leaving the shadow cone as there are second layer atoms. The shadow edge position is thus dominated by the edge of the shadow of the second layer on the third. Therefore, derivation of δ from this shadow edge is not straightforward and cannot be done using our method of data analysis.

However, if the detector is put in the [101] blocking direction, and if the surface is reconstructed according to the missing row model, only those ions which are scattered by the first layer and by half of the second layer can reach the detector; third layer scattering is blocked by second layer atoms. We studied the $[\bar{2}11]$ shadow with the detector put in that blocking direction, turned out of the plane of incidence over an angle $\Delta = 59°$.

To show the relevance of this combination of shadowing and blocking techniques, two polar angular distributions are taken in the $[\bar{3}32]$ azimuth to study the $[\bar{2}11]$ shadow, one on the clean surface (fig. 14, solid line) and one on the oxygen-covered surface (dashed line). The solid line exhibits no visible $[\bar{2}11]$ edge at $\psi = 30°$, but the dashed line does. If the surface were to be reconstructed according to the shifted row model, no sharp edge would be observed, so this model can safely be ruled out.

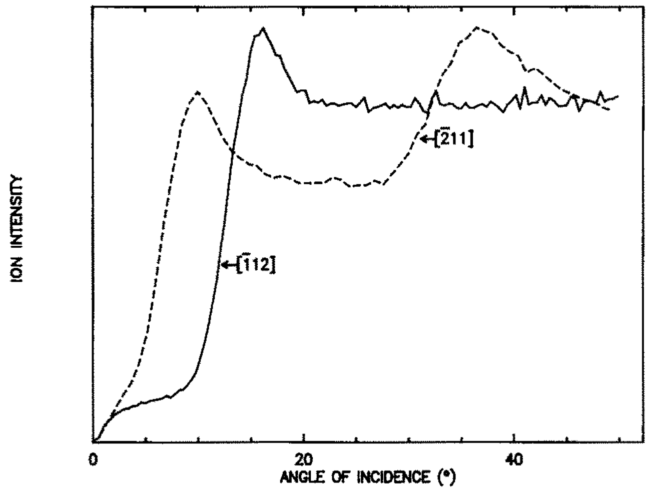

Fig. 15. Polar angular distribution represented by the solid line is taken on the clean surface in the $[\bar{1}12]_s$ direction and the other distribution is taken on the oxygen-covered surface in the $[\bar{2}21]_s$ direction. The geometry is chosen in such a way that yield from the third layer and deeper cannot reach the detector when the beam is aimed along the $[\bar{2}11]$ direction ($\Theta = 124°$, $\Delta = 59°$).

The same procedure and analysis as applied to the clean surface can now be applied to the oxygen-covered surface if the combination of shadowing and blocking just described is used. Fig. 15 shows the polar angular distributions measured in the $[\bar{1}12]_s$ and $[\bar{3}32]_s$ directions. The distribution in the $[\bar{1}12]_s$ direction is measured on the clean copper surface and the distribution in the $[\bar{3}32]_s$ direction is measured on the oxygen covered surface. The angular widths of these two distributions are equal within 0.2°, indicating that we are not dealing with a mixture of shadows.

If the surface were to be reconstructed according to the ST model, the shadow edge would be broadened, because the ions scattered by half of the third layer would be able to reach the detector without being blocked, just as they did in the case discussed above, where the detector was not put in the blocking direction. But the two distributions shown in fig. 15 have an edge of equal width, so the ST model can be ruled out too.

In all the reconstruction models, except the SR model, the distance between two neighbouring copper surface atoms in the $[\bar{1}10]_s$ direction is twice as large as the corresponding bulk value, namely 5.112 Å. The experimentally found critical angle in a polar angular distribution in this surface direction agrees within 0.2° with the calculated value, as can be seen in table 2, if it is assumed that the distance between the two copper atoms is 5.112 Å. The agreement is poor if this distance is assumed to be approximately 2.55 Å.

In our experimental data, we have found evidence against the SR and ST models but not against the MR model. Bonzel and Ferrer [15] have argued that the MR model is not possible, because starting from an unreconstructed surface the copper atoms have to move over distances, large compared to the lattice distance if the surface structure is to correspond to the MR model. However, another reconstruction model is possible, which is not in conflict with our experimental data and the SEXAFS measurements and in which the copper atoms do not have to move over large distances. In this model the initial adsorption site of the oxygen atoms is in the $[\bar{1}10]$ rows, where the electron density is highest. Second layer copper atoms move in the [010] direction to a position above the surface in the neighbourhood of the oxygen atom, and form a new [001] row. In this model the new second layer is complete, just as in the MR model. The newly formed first layer and the third layer have the same configuration; both lack every second [001] row. The surface configuration formed in this way is deeply grooved, so we call this configuration the grooved surface (GS) model. Because we have not found any arguments in our experimental data for preferring the GS model over the MR model, we will use the MR model in the remainder of this article.

To obtain a value for the relaxation we analysed the two distributions of fig. 15 on the basis of relation (2). The critical angles of the $[\bar{2}11]$ and $[\bar{1}12]$ shadow edges were found to be 31.6° and 12.0°, respectively. Using these values, we found that the distance between the first and second copper layer is increased by 0.23 ± 0.04 Å, (18 ± 3)%. This value is in agreement with the first estimation of this value given by Hupkens [30], 1.6 ± 0.3 Å, who performed LEIS measurements with 4 keV Ne^+ projectiles. It is in good agreement with the value obtained by Yarmoff et al. [8], who performed ICISS measurements with 3 keV Li^+ projectiles. These authors found (25 ± 10)%. They also concluded that the missing row model is the correct one. Our distributions measured on the oxygen-covered surface are of the same quality as the distributions measured on the clean surface, so the uncertainty in the value for the relaxation is the same in both cases.

5.3. The position of the oxygen

In order to obtain a value for the vertical position of the oxygen above or below the first layer, we analysed the shadow of the copper atom on the oxygen atom in the $[\bar{2}21]_s$ direction, as seen in the oxygen recoil photogram. The energy of the oxygen recoil atoms at the edge of the shadow cone differs considerably from the pure binary collision recoil energy. The recoil energy in a binary collision is given in relation (3), in which A is the ratio of the oxygen mass to the neon mass:

$$E_{rec} = E_0\left[4A/(A+1)^2\right]\cos\Theta \simeq E_0\cos^2\Theta. \qquad (3)$$

The relative energy shift can be defined as:

$$\frac{\mathrm{d}E}{E\,\mathrm{d}\Theta}\Delta\Theta = 2\tan(\Theta)\Delta\Theta. \tag{4}$$

In this relation $\Delta\Theta$ represents the angle by which the neon ions are deflected by the first copper atom. The energy loss caused by this deflection is negligible. The distance between the copper atom and the oxygen atom is 5.4 Å, for all proposed positions for the oxygen in the literature. It can be calculated that the neon ions scattered at the edge of the shadow cone, 5.4 Å away from the first copper atom, are deflected over $\Delta\Theta = 2.3°$ by the first copper atom. Using this value for the deflection, one can calculate the energy shift. The detection angle is 55° so the energy shift is 11%, which is considerably higher than the energy resolution of the analyser and also much higher than the shifts listed in table 2.

In order to eliminate the influence of the energy shift in measurements of the shadow edge in recoil angular distributions, we determined the peak area in energy spectra. Each data point in a polar angular distribution now represents the integration of a part of an energy spectrum instead of a single data point in it. In this way the size of the energy shift does not influence the position of a shadow edge in a polar angular distribution.

Two polar angular distributions are measured: one distribution of reflected neon ions around the $[\bar{1}12]$ shadow edge ($\Theta = 100°$) measured on the clean surface and one distribution of oxygen recoils ($\Theta = 55°$) measured in the $[\bar{2}21]_s$ direction. The position of the $[\bar{1}12]$ shadow edge in the first distribution differs by only 0.4° from the value found in a "normal" polar angular distribution. Comparison of these two types of distributions for the shadow of copper on oxygen yields an angular difference of 1.4°.

Comparison of these two shadows, obtained by evaluating peak areas, shows that the oxygen is 0.1 ± 0.1 Å *below* the surface. Both distributions are drawn in fig. 16. The possible error in the value thus found is higher than the uncertainty in the determination of the relaxation of the surface. This is mainly caused by the uncertainty in the determination of the background intensity (0.3°) and by the uncertainty in the potential between the oxygen atoms and neon atoms (0.04 Å). The angular width of both distributions in fig. 16 is 1.3°.

In fig. 13a, a shadow in the $[\bar{1}00]$ direction is observed. This area of low ion intensity is caused not only by a shadow of the first layer on the third, but also by a shadow of the oxygen atoms on second layer copper atoms. The critical angles calculated using our values for the distance between the two topmost layers and for the position of the oxygen and assuming a bulk value for the distance between the second and third copper layer are 60.0° and 62.4° respectively. The uncertainty in the latter value is large because of uncertainty in the potential between the neon and the oxygen atoms. The experimentally

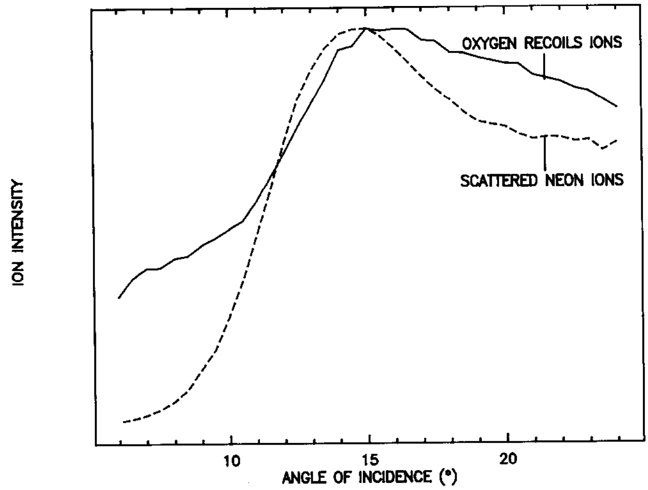

Fig. 16. Two polar angular distributions. Each data point represents the integration of a part of an energy spectrum. The oxygen recoil distribution is measured in the $[\bar{2}21]_s$ direction ($\Theta = 55°$, $\Delta = 0°$) and the neon ion distribution in the $[11\bar{2}]_s$ direction ($\Theta = 100°$, $\Delta = 0°$).

found critical angle in a polar angular distribution is 60.4°. Because these two shadows are close to each other, no experimental values can be obtained from our data for the distance between the first layer and the third layer.

6. Conclusions and summary

In this article, the LEIS method as applied by us has been outlined and critically analysed. In addition, results concerning the atomic surface configuration of the clean and oxygen-covered Cu(110) surface have been presented. Regarding the LEIS method we can conclude the following:

- Above a projectile energy of 4 keV and a scattering angle of 70°, the ion fraction of neon ions scattered by a Cu(110) surface can reach values of up to 40%. Small trajectory changes do not influence the ion fraction. In a polar angular distribution between two shadow edges within the relevant range of polar angles of incidence the ion intensity is almost constant.
- If the experimental conditions are appropriately chosen, one can suppress deeper layer and multiple scattering contributions by using Ne^+ scattering instead of using alkali ions or neutralised noble gas ions. Another advantage of using Ne^+ ions over alkali ions is that they do not contaminate the surface.
- There is no need to choose scattering angles close to 180° (ICISS). At smaller scattering angles as well, the influence of blocking is small. In

addition, at a somewhat smaller Θ the scattering cross section and thus the ion yield is higher, which allows us to use low doses.

- If the copper surface is studied with neon ions, there is no need for complicated computer simulations because of the high surface sensitivity.

Regarding our results for the surface structure we conclude the following:

- The clean Cu(110) surface is somewhat contracted (3 ± 3)%. This value is at the lower end of the results previously published in the literature.
- The oxygen-covered surface is not reconstructed according to the shifted row or the saw-tooth model. No evidence was found for rejecting the missing row model.
- A combination of shadowing and blocking techniques permits us to determine the distance between the two topmost copper layers of the oxygen covered copper surface. This surface was found to be relaxed over 0.23 ± 0.04 Å. This value is in agreement with the only other result we have found in the literature.
- For the vertical position of the oxygen the analysis of polar angular distributions in the $[\bar{2}21]_s$ direction yields a value of 0.1 ± 0.1 Å below the surface.
- The distances between the adsorbed oxygen atoms and their first and second neighbouring copper atoms, resulting from these data, are 1.81 ± 0.01 Å and 1.90 ± 0.09 Å respectively. This is in agreement with results of SEXAFS measurements [6] which yield 1.81 ± 0.02 Å for the first nearest neighbour distance, and 1.97 ± 0.02 and 1.99 ± 0.02 Å for the second nearest neighbour distance. We emphasize, however, that the vertical oxygen position, derived indirectly from the SEXAFS results, as being above the first Cu layer, disagrees with our direct result. This discrepancy arises because the SEXAFS results were evaluated on the assumption of an unrelaxed first to second layer distance whereas according to our measurements a relaxation by 0.23 ± 0.04 Å occurs.

Acknowledgements

This work was performed as part of the research programme of the "Stichting voor Fundamenteel Onderzoek der Materie" (FOM) with financial support from the "Nederlandse Organisatie voor Wetenschappelijk Onderzoek" (NWO).

References

[1] A.G.J. de Wit, R.P.N. Bronckers and J.M. Fluit, Surface Sci. 82 (1979) 177.
[2] R.P.N. Bronckers and A.G.J. de Wit, Surface Sci. 112 (1981) 133.

[3] J. Lapujoulade, Y. le Cruer, M. Lefort, Y. Lejay and E. Maurial, Phys. Rev. B 22 (1980) 5740.

[4] J. Lapujoulade, Y. le Cruer, M. Lefort, Y. Lejay and E. Maurial, Surface Sci. 118 (1982) 103.

[5] U. Döbler, K. Baberschke, J. Haase and A. Puschmann, Phys. Rev. Letters 52 (1984) 1437.

[6] M. Bader, A. Puschmann, C. Ocal and J. Haase, Phys. Rev. Letters 57 (1986) 3273.

[7] H. Niehus and G. Comsa, Surface Sci. 140 (1984) 18.

[8] J.A. Yarmoff, D.M. Cyr, J.H. Huang, S. Kim and R.S. Williams, Surface Sci. 165 (1986) L73.

[9] U. Döbler, K. Baberschke, D.D. Vvedensky and J.B. Pendry, Surface Sci. 178 (1986) 679.

[10] R. Feidenhans'l and I. Stensgaard, Surface Sci. 133 (1983) 453.

[11] R.A. Didio, D.M. Zehner and E.W. Plummer, J. Vacuum Sci. Technol. A 2 (1984) 852.

[12] J.M. Mundenar, A.P. Baddorf, E.W. Plummer, L.G. Sneddon, R.A. Didio and D.M. Zehner, Surface Sci. 188 (1987) 15.

[13] W. Sesselmann, H. Conrad, G. Ertl, J. Küppers, B. Woratschek and H. Haberland, Phys. Rev. Letters 50 (1983) 446.

[14] G. Ertl, Surface Sci. 6 (1967) 208.

[15] H.P. Bonzel and S. Ferrer, Surface Sci. 118 (1982) L263.

[16] J.M. van Zoest, Thesis, Utrecht (1986).

[17] E.S. Mashkova and V.A. Molchanov, in: Medium-Energy Ion Reflection from Solids (North-Holland, Amsterdam, 1985) p. 30.

[18] Th. Fauster and M.H. Metzner, Surface Sci. 166 (1986) 29.

[19] M. Aono, Nucl. Instr. Methods B 2 (1984) 374.

[20] W. Hetterich, H. Derks and W. Heiland, Appl. Phys. Letters 52 (1988) 371.

[21] D.L. Adams, H.B. Nielsen and J.N. Andersen, Surface Sci. 128 (1983) 294.

[22] D.L. Adams, H.B. Nielsen and J.N. Andersen, Phys. Scripta T 4 (1983) 22.

[23] H.L. Davis, J.R. Noonan and L.H. Jenkins, Surface Sci. 83 (1979) 559.

[24] J.R. Noonan and H.L. Davis, Surface Sci. 99 (1980) L424.

[25] H.L. Davis and J.R. Noonan, Surface Sci. 126 (1983) 245.

[26] I. Stensgaard, R. Feidenhans'l and J.E. Sørensen, Surface Sci. 128 (1983) 281.

[27] D.L. Adams, H.B. Nielsen, J.N. Andersen, I. Stensgaard, R. Feidenhans'l and J.E. Sørensen, Phys. Rev. B 49 (1982) 669.

[28] M. Copel, T. Gustafsson, W.R. Graham and S.M. Yalisove, Phys. Rev. B 33 (1986) 8110.

[29] Th. Fauster, Vacuum 38 (1988) 129.

[30] Th. M. Hupkens, Thesis, Utrecht (1983) p. 75.